

# Time resolution of Burle 85001 micro-channel plate photo-multipliers in comparison with Hamamatsu R2083.

V. Baturin<sup>a</sup>, V. Burkert<sup>b</sup>, W. Kim<sup>a</sup>, S. Majewsky<sup>b</sup>,  
D. Nekrasov<sup>a</sup>, K. Park<sup>a</sup>, V. Popov<sup>b</sup>, E.S. Smith<sup>b</sup>, D. Son<sup>a</sup>,  
S.S. Stepanyan<sup>a</sup>, C. Zorn<sup>b</sup>.

<sup>a</sup>*Kyungpook National University, Daegu 702-701, Republic of Korea.*

<sup>b</sup>*Thomas Jefferson National Accelerator Facility, Newport News, Virginia  
23606, USA*

---

## Abstract

The CLAS detector will require improvements in its particle identification system to take advantage of the higher energies provided by the Jefferson Laboratory accelerator upgrade to 12 GeV. To this end, we have studied the timing characteristics of the micro-channel plate photo-multiplier 85001 from Burle, which can be operated in a high magnetic field environment. For reference and comparison, measurements were also made using the standard PMT *R2083* from Hamamatsu using two timing methods. The cosmic ray method, which utilizes three identical scintillating counters  $2 \times 3 \times 50 \text{ cm}^3$  with PMs at the ends, yields  $\sigma_{R2083} = 59.1 \pm 0.7 \text{ ps}$ . The location method of particles from radiative source with known coordinates has been used to compare timing resolutions of *R2083* and *Burle* – 85001. This “coordinate method” requires only one counter instrumented with two PMs and it yields  $\sigma_{R2083} = 59.5 \pm 0.7 \text{ ps}$  in agreement with the cosmic ray method. For the micro-channel plate photomultiplier from Burle with an external amplification of 10 to the signals, the coordinate method yields  $\sigma_{85001} = 130 \pm 4 \text{ ps}$ . This method also makes it possible to estimate the number of primary photo-electrons.

---

PACS:

Keywords: CLAS, JLAB, time-of-flight, time resolution, micro-channel plate, MCP photomultiplier.

---

\* Corresponding author: Wooyoung Kim (wooyoung@jlab.org).

## 1 Introduction

The CEBAF electron accelerator at Jefferson Lab in Newport News, Virginia, is dedicated to exploring the nature of strongly interacting matter. The Department of Energy has recently affirmed the decision to double the current energy of the machine to 12 GeV by giving CD-0 approval to the 12 GeV upgrade project[1]. The increased energy reach of the machine will open up new opportunities in hadronic physics, as well as new challenges. The experimental equipment will be upgraded to take advantage of the higher beam energies, since both the momenta and multiplicity of secondary particles will be significantly higher. Therefore the particle identification criteria and space-time resolution, as well, has to be improved.

The current time-of-flight (TOF) system[2] is the primary tool for hadron identification in the CLAS detector. The upgraded CLAS uses Cerenkov light as well as TOF for hadron identification. The new TOF system[1] will have a refurbished forward-angle detector, and a barrel scintillation detector for triggering and time-of-flight measurements in the central region. The present work concentrates on studies which are of special interest to the barrel detector.

The nominal barrel geometry consists of 50 scintillating “time-zero” counters each 50 cm long and  $2 \times 3 \text{ cm}^2$  in cross section. These counters will be placed inside the superconducting solenoid at a 25 cm radius from the beam axis. One of the goals of the CLAS upgrade program for the barrel counters is to achieve a timing resolution  $\sigma_{TOF} \approx 50 \text{ ps}$ , which will allow the separation of pions from kaons up to 0.64 GeV/c and pions from protons up to 1.25 GeV/c.

The TOF counters of CLAS[2] have two PMTs, one at each end of scintillation counters. Therefore, assuming the PMTs have the same resolution, one can determine the TOF resolution between two counters as  $\sigma_{TOF} = \sigma_{PMT}$ . However, if the TOF is measured relative to the precise radio frequency (RF) signal of the accelerator, then  $\sigma_{TOF} = \frac{1}{\sqrt{2}}\sigma_{PMT}$  since the RF jitter may be neglected. Thus we aim to construct a time-zero counter with the effective resolution  $\sigma_{PMT} \leq \sqrt{2} \times 50 \text{ ps}$ . We refer to  $\sigma_{PMT}$  as an “effective resolution” in order to emphasize that this value is defined not only by the excellent characteristics of PMTs we use in our tests, but by the experimental environment, as well. In particular, the barrel structure of 50 time-zero scintillators is expected to be placed in the area of a high magnetic field  $B \approx 2 \text{ T}$ , and high counting rate. Both of these can influence the photomultiplier signals and deteriorate the timing resolution. If ordinary dynode photomultiplier tubes (PMTs) are used, then the only option is to move the PMTs out of the region of high magnetic field, which requires bent light guides that are at least a meter long to transport the scintillator light to reduced field locations.

An alternative solution would be the implementation of micro-channel plate (MCP) PMs, which were first tested as components of a scintillation time-of-flight system[4] with resolution of  $\approx 400ps$ . Due to obvious immunity of MCPs to magnetic fields[5], which was verified up to  $2T$ , micro-channel plate PMs could be attached directly to scintillators. Since the MCP transition time is short, the single electron resolution of MCP may in principle be as low as  $\approx 30 ps$ [5]. Unfortunately the resolution of scintillation counters is mostly dictated by statistical fluctuations in the number of photo-electrons, and therefore reduced quantum efficiency will have a direct adverse effect on timing.

In this paper we evaluate the possibilities of achieving the goals for the TOF barrel for the upgraded CLAS12 detector. To this end we have conducted tests using cosmic rays and a  $^{90}Sr$  radioactive source to study the resolution of scintillation counters (Bicron BC-408) with two PMTs on each. Various tests required up to three identical counters, each  $2 \times 3 \times 50cm^3$  in size. First we instrumented the setup with standard fast  $R2083$  from Hamamatsu. The time resolution of  $R2083$  PMTs was determined with a standard cosmic-ray setup using three identical counters. The radiative source and one of these counters was used to check the measurements with the “coordinate method” described below. Then we replaced the fast  $R2083$  PMTs by MCP PMs “Burle-85001” in the test counter and repeated the study with the ionization source. We also made measurements of the number of photoelectrons detected, and rate capability of the counters which are of general interest to the program.

In Section 2 we describe two methods measuring  $\sigma_{PMT}$ . Applications of these methods to conventional PMTs are described in Section 3. Results for MCP PM 85001 from Burle are presented in Section 4.

## 2 Methods for the measurements of PMT resolution.

Historically, cosmic-rays have been a useful tool for studying the timing resolution of minimum ionizing tracks in test setups [4]. We have used this procedure as a benchmark, and for checking the consistency of a simpler and quicker method, “coordinate method,” detailed below. First we review the technique for completeness. It requires at least two identical counters, but we use a more robust method using three stacked parallel equidistant counters instrumented with 6 identical PMs. The experimental setup and electronics circuit diagram are shown in Fig. 1. To discriminate the PMT signals we use constant fraction discriminators ORTEC-935. The signals were divided equally at the inputs to the discriminators. One part was used for discriminating at the threshold  $\approx 20 mV$ , while the second part was fed to ADC inputs. The arrival times  $t_{1,\dots,6}$  of the discriminated signals relative to one of PMTs were digitized by

LeCroy-2228A TDCs. The corresponding pulses were integrated ( $a_{1,\dots,6}$ ) within a 200 ns gate by LeCroy-2229 ADCs.

**The method of cosmic ray tracking.** The times  $t_{t,m,b}$  due to light flashes in the top, middle and bottom- counters, respectively, are defined as:

$$t_t = (t_1 + t_2)/2; \quad t_m = (t_3 + t_4)/2; \quad t_b = (t_5 + t_6)/2, \quad (1)$$

where  $t_{i=1-6}$  are the corresponding TDC readout values. The longitudinal coordinates of the particle track  $x_{t,m,b}$  we determine as

$$x_t = (t_1 - t_2)/2; \quad x_m = (t_3 - t_4)/2; \quad x_b = (t_5 - t_6)/2. \quad (2)$$

Thus the track may be reconstructed and straight trajectories may be selected. For straight tracks the following relation between ideally measured  $t_{t,m,b}$  holds:

$$t_r = t_m - (t_t + t_b)/2 = 0. \quad (3)$$

However, since  $t_{t,m,b}$  are smeared by PMT resolution, the value  $t_m - (t_t + t_b)/2$  jitters around zero, as well. Hence, the method is based on the statistical analysis of residuals of Eq.3:

$$\delta t_r = \delta \left( (t_1 + t_2)/4 - (t_3 + t_4)/2 + (t_5 + t_6)/4 \right). \quad (4)$$

Keeping in mind that one of the PMTs has been used for the common start ( i.e. the corresponding  $\delta t = 0$ ), from Eq.4 we estimate the effective PMT resolution as

$$\sigma_{PMT} = \sqrt{\text{var}(t_i)} = \sqrt{\frac{16}{11}} \sqrt{\text{var}(t_r)}. \quad (5)$$

**Coordinate method.** In order to be able to perform measurements of the effective PMT resolution quickly, we have developed the so-called ‘‘coordinate method.’’ This method requires only one scintillating counter with two identical PMTs attached to its ends. The resolution of the PMTs was determined from the residuals of measured coordinates of ionizing  $\beta$ -particles from a radiative  $^{90}\text{Sr}$  source. The distribution of  $\beta^-$  in the collimated beam was derived from the counting rate profile [6] of the source. The latter was measured with our scintillator by moving the source in 1 mm steps across the scintillator and then differentiated. The resulting distribution was fit with the Gaussian

of  $\sigma_{beam} \approx 3 \text{ mm}$ . Such small beam size may be taken into account or even neglected.

The coordinate method is based on the simple relation between the position  $x$  of the source along the counter and arrival times,  $t_l$  and  $t_r$ , of signals at the two PMTs located at the ends of the scintillator:

$$t_x = t_l - t_r = \frac{2x}{c_s} + const. \quad (6)$$

where  $x$  is the coordinate of the light flash,  $t_x$  is the time interval measured with TDC,  $c_s \approx 13.5 \text{ cm/ns}$  is the effective speed of light in scintillating media, the constant *const* accounts for all kinds of propagation delays. For convenience we define  $X = x/c_s$  which measures position in units of time.

The variance of  $t_x$  can be related to the PMT resolution  $\sigma_{PMT}$  through the relation

$$var(t_x) = var(t_l) + var(t_r) + var(t_{TDC}) + \left(\frac{2}{c_s}\right)^2 var(x) \quad (7)$$

where  $var(t_{l,r})$  are the variances for left or right PMTs. We assume that  $\sigma_{PMT}^2 = var(t_l) = var(t_r)$ ; the value  $var(t_{TDC}) \approx (25 \text{ ps})^2$  is the resolution of the TDC measurements, and  $var(x) \approx (15 \text{ ps})^2$  represents the size of the irradiating beam. Thus, from this formula one can determine the single PMT resolution as

$$\sigma_{PMT} = \frac{1}{\sqrt{2}} \sqrt{var(t_x) - var(t_{TDC}) - \left(\frac{2}{c_s}\right)^2 var(x)} \approx \frac{1}{\sqrt{2}} \sigma_{t_x}, \quad (8)$$

where the rightmost term is obtained neglecting the beam size and TDC resolution. We illustrate the coordinate method in Fig. 2, in which we show two images of the radiative source. These images were accumulated in two energy intervals of  $\beta^-$ -particles, where the longitudinal coordinates along the counter were determined via Eq. (6). The 50 cm wide plateau is the manifestation of cosmic particles spanning by the counter. The two peaks at about zero are due to the ionization source placed at the center of the counter.

From the data in Fig. 2 one can obtain a first estimate of the resolution for minimum ionizing particles(MIP). We determined the width of the peak in the bottom panel of this figure  $\sigma_x = 1.18 \text{ cm}$ . From Eqs. 6 and 8 we find  $\sigma_{PMT}(1.2 \text{ MeV}) = \sqrt{2} \times \sigma_x / c_s = 123 \text{ ps}$ . The energy average deposited by MIPs is 4.4 MeV in our 2cm thick scintillator. Therefore, since  $\sigma_{PMT} \propto \frac{1}{\sqrt{E}}$ , the expected  $\sigma_{PMT}(E_{MIP}) \approx \sqrt{\frac{4.4}{1.2}} \sigma_{PMT}(1.2) = 64.2 \text{ ps}$ . We present this rough estimation to demonstrate the transparency of the method. However,

for measuring the effective  $\sigma_{PMT}$  we use the more rigorous coordinate method, extrapolated to the energy of MIP, which we describe below.

**Coordinate method with extrapolation of  $\sigma(E_\beta)$  to  $\sigma_{PMT}(E_{MIP})$ .** From the off-line analysis of data files accumulated with the radiation source we determine the dependence of the PMT resolution upon the energy of  $\beta$ -particles. The typical outcome of such study with  $^{90}\text{Sr}$  source is shown in Fig. 3. This figure contains plots for the source location at  $-15\text{ cm}$ . Below we explain the contents of each panel.

The energy( $E$ ) spectra (Fig. 3 top-left) of  $\beta$ -particles from the  $^{90}\text{Sr}$  source was determined using

$$E = k\sqrt{(a_l - p_l)(a_r - p_r)} \quad (9)$$

where  $a_{l,r}$  and  $p_{l,r}$  are the amplitudes and pedestals from  $ADC$ s corresponding to left or right sides of the counter;  $k$  is the calibration constant. The latter has been determined from the fit of  $\beta$ -spectrum parameterized by

$$n(\varepsilon) = G(\varepsilon) \times \varepsilon\sqrt{(\varepsilon^2 - 1)}(\varepsilon_0 - \varepsilon)^2 \quad (10)$$

where  $\varepsilon = E/m_e c^2$ ,  $n(\varepsilon)$  is the number of events with specified  $\varepsilon$ ,  $\varepsilon_0 = 2.28\text{ MeV}/m_e c^2$  is the upper limit of  $\beta$ -spectrum for  $^{90}\text{Sr}$ ,  $G(\varepsilon)$  is an empirical smoothing function.

The measured distribution of the longitudinal coordinate  $X$ , defined by Eq. 6, is shown in Fig. 3 bottom-left. The peak at zero is the image of the source. Such distribution can be plotted for a narrow slice in measured energy (100  $keV$  wide), as well. In order to determine  $\sigma_X(E)$ , we create a scatter plot  $X$  vs  $E$  via aforementioned slices. The energy dependence of the centroid of the source image  $\langle X \rangle(E)$  is determined by the above procedure and plotted in Fig. 3 bottom-right. The width of the position distribution in each energy slice gives the measured dependence of  $\sigma_X(E)$  and is plotted in Fig. 3 top-right. As one can see from the plot, the data for  $E < 2.3\text{ MeV}$  is well-described by a  $1/\sqrt{E}$  behavior, apparently due to the increase of the number of photons. Extrapolating  $\sigma_X(E)$  to the energy deposit of minimum ionizing particles  $4.4\text{ MeV}$  we estimate  $\sigma_{MIP} = 63.9 \pm 1.5\text{ ps}$ .

**Measurements of the number of primary photo-electrons.** The following method has been used for estimating the number of primary photo-electrons. We define two energies *measured* from two sides of the counter:

$e_{l,r}(E) = k_{l,r} \times (a_{l,r} - p_{l,r})$ , where  $k_{l,r}, a_{l,r}, p_{l,r}$  are the corresponding calibrating factors, ADC values and pedestals, respectively; obviously  $e_{l,r}(E) \propto E$ . We determine the total energy  $e$  and the difference  $\Delta e$  as

$$e(E) = (e_l + e_r) \propto E \quad \text{and} \quad \Delta e(E) = e_l - e_r. \quad (11)$$

For the standard deviations of both values, defined above, we write

$$\sigma_{\Delta e}^2 = \text{var}(e_l) + \text{var}(e_r) = \sigma_e^2. \quad (12)$$

Since  $\sigma_e^2 \propto N(E)$ , where  $N(E)$  is the fluctuating number of primary photoelectrons in *both* PMTs, we find

$$\frac{\sigma_e}{e} = \frac{\sqrt{N(E)}}{N(E)}. \quad (13)$$

Thus the energy dependent number of primary photoelectrons may be determined as

$$N(E) = \left( \frac{e(E)}{\sigma_e(E)} \right)^2 = \left( \frac{e(E)}{\sigma_{\Delta e}(E)} \right)^2 \quad (14)$$

A special procedure is required to measure  $\sigma_e$  with the continuous energy spectrum. However, the function  $\sigma_{\Delta e}(E)$  may be derived from the slices of the scatter plot  $\Delta e$  vs  $E$ . Using the fact that  $\sigma_{\Delta e} = \sigma_e$  (Eq. 12) we estimate  $N(E)$  via Eq. 14 and extrapolate this function to MIP's energy. Thus measured  $N(E) = 685 \pm 10$  and its extrapolation to the MIP energy of 4.4 MeV is shown in Fig. 4. This number of primary photo-electrons collected in our  $2 \times 3.3 \times 50 \text{ cm}^3$  scintillator is comparable to the number of  $1000 \pm 100$  determined for TOF counters of CLAS[2] with a size of  $5.1 \times 15 \times 32.3 \text{ cm}^3$ . In our case, the number of primary photo-electrons is supposed to be emitted from *two* photo-cathodes, the sensitivity of which in R2083 is  $\approx 80 \mu\text{A}/\text{lm}$ . The value  $1000 \pm 100$  relates to *one* photo-cathode of *EMI - 9954B* photo-multiplier with the sensitivity of  $\approx 110 \mu\text{A}/\text{lm}$ .

**Advantages of the coordinate method.** The coordinate method has several important advantages. Firstly, it requires only one counter instrumented with two identical PMTs. Secondly, the data taking and data analysis up to the final value takes only several minutes. Finally, this method is insensitive to the systematics related to the coordinate dependence of signal's timing, since the ionization is localized in the known narrow region of  $\pm 0.3 \text{ cm}$ . Moreover, the coordinate method may be used for studies of the coordinate dependent

systematics, which may be measured directly at different locations of the ionizing source.

### 3 Measurements of time resolution.

To discriminate the PMT signals we use the constant fraction discriminators ORTEC-935. The signals were divided equally at the inputs of discriminators. One part was used for discriminating at the threshold  $\approx 20$  mV, while the second part was fed to ADC inputs. The arrival times of the discriminated signals relative to one of PMTs were digitized by the LeCroy-2228A TDC. The corresponding pulses were integrated within 200 ns gate by the LeCroy-2229 ADC.

**Study of  $\sigma_{R2083}$  vs PMT gain via the coordinate method.** We have measured the dependence of  $\sigma_{PMT}$  on the PMT gain, which is obviously proportional to the average amplitude of output signals. The HVs of both PMTs were tuned to provide amplitudes from both sides to be equal. The dependence of the resolution upon the amplitudes of signals is shown in Fig. 5. One can see that the resolution gradually improves up to the averaged signal amplitude of 900 mV. Above this value the resolution is almost constant.

**Study of  $\sigma_{PMT}$  vs position along the counter.** In order to study the systematics of PMT timing we have measured the  $X$ -dependence of both the peak location and  $\sigma_{PMT}$ . In advance we have equalized signals from both sides at the center of the counter. The dependence of the resolution upon  $x$ -coordinate of the source is shown in Fig. 6. The measured resolution oscillates near the mean value of  $59.5 \pm 0.7$  ps.

**Cosmic-ray tracking and comparison of coordinate method.** The result from the three counter tracking method is shown in Fig. 7. The local resolution has been determined to be of  $59.1 \pm 0.7$  ps. The overall resolution yielded by this method is of  $63.4 \pm 0.6$  ps. The last value is worse due to some  $x$ -dependent displacement of residuals, which may be seen in Fig. 7 bottom-right.

Thus, we consider that the coordinate method is well established. It yields values which agree nicely with the tracking method applied to cosmic particles. Therefore, this quick method may be trusted for studies of timing resolution of various photo-multipliers.

#### 4 Resolution, counting rate, and number of photo-electrons for MCP PMs.

We have implemented the coordinate method to measure the resolution of Micro-channel Plate PMs “Burle-85001-501” with the same scintillator and setup. However, an amplifier (*LeCroy* – 612A) was required for these measurements, since signals from the MCPs are too small for discriminating. We note that the sensitive surface of the “Burle-85001-501” assembly is formed by four MCPs. First we performed the resolution tests with four MCPs connected to the input circuit in parallel. Then we repeated our tests with only one of four MCPs feeding the input circuit. We find no difference between two measurements. Thus the individual transition times and deviations may be considered equal. We emphasize that according to its data sheet the photocathode sensitivity of *Burle* – 85001 – 501 lies between 40 and 55  $\mu\text{A}/\text{lm}$ . This value is about twice lower than that for *R2083* PM. Therefore the number of primary photoelectrons has to be at least twice lower and one can expect the timing resolution of MCP PM to be of  $\sqrt{2}$  times worse.

The resulting plots of coordinate method with MCP PM are shown in Fig. 8. The method yields  $\sigma_{PMT} = 125 \pm 4$  for MIPs. This value is almost twice the resolution of the *R2083*. Since the single electron resolution of MCP is very good then the reasons for the worse resolution could be: (1) noise of preamplifier, (2) increased effects of statistical fluctuations of primary photoelectrons. The first assumption will be checked in future measurements with an “on-board” preamplifier, such as that described in Ref. [7]. We checked the second possibility by measuring the number of primary photoelectrons.

**Number of primary photoelectrons in the MCP.** We have measured the number of primary photoelectrons produced by M.I.Ps using the same method as for the PMs from Hamamatsu. The resulting distributions are shown in Fig. 9. The extrapolated  $N_{ppe}(4.4 \text{ MeV})$  (for *two* MCPs) was found to be of  $127 \pm 10$ . This value is 5.4 times lower compared to the *R2083* photomultiplier and about 2.7 times lower than expected from the data sheet value. We note that  $\frac{\sigma_{85001}}{\sigma_{R2083}} \approx 2.2$ , which agrees with the ratio of corresponding  $\sqrt{N_{ppe}}$  numbers(2.3). Thus, our measurements look consistent.

**Measurements of MCP gain.** The MCP gain was determined using the measured  $N_{ppe}$  and the charge spectra of  $\beta$ -particles measured by ADCs with the source at the center of the counter. We can thus plot the measured gains as function of the MCP voltages, as shown in Fig. 10. We remind the reader that the voltages have been tuned to provide equal amplitudes from two sides of the detector.

**Timing resolution vs MCP gain.** We have measured the effective resolution of MCP PMs at different high voltage settings and amplification factors  $10^0, 10^1, 10^2$  cascading our preamplifier's. The resolution yielded by coordinate method is shown in Fig. 11 as a function of the MCP gain. One can see a plateau between gains  $0.4 \times 10^5$  and  $6.5 \times 10^5$ , where the extrapolated resolution lies in the interval  $(102, 132)$  ps. The leftmost and rightmost points in this figure were obtained at very low output signals (below  $5pC$ ) with the amplification factors of  $10^2$  and  $10^0$ , respectively. Therefore we exclude them from consideration.

**Counting rate capability of MCP PM with Light Emitting Diode.**

The counting rate capability of 85001 PM has been measured in the following way. The radiative source was replaced by a Light Emitting Diode. This LED was fed from the pulser *LeCroy* – 9210 with a pulse of  $5V$  amplitude and controllable width  $50 < \tau < 100$  ns. From the scope measurements the rise time of the light signal was found to be equal to  $\tau$ , while the amount of light produced by LED  $\propto \tau^2$ .

We tested the counting rate capability at MCP gains of approximately  $6.5 \times 10^5$  and  $6.5 \times 10^4$ . At high gain we have also taken data at *high* and *low* intensities of light flashes, corresponding to  $\tau=100$  ns and  $50$  ns, respectively. The behavior of signal charge vs counting rate is shown in Fig. 12. From curves (1) and (2) in this figure one can conclude that indeed the signal charge is proportional to  $\tau^2$ . The plateau region of curve (3), obtained with *low* gain  $\approx 0.65 \times 10^5$ , is significantly wider than that of curve (1) at *high* gain  $\approx 6.5 \times 10^5$ . From Fig. 11 we find that  $\sigma_{85001} \approx 130$  ps at gain  $\approx 0.65 \times 10^5$ .

Hence, one can conclude that at *low* gain, with an amplification factor of  $10^2$ , the MCP PM can operate with a resolution of  $\approx 130ps$  and at counting rates up to  $0.5 \times 10^6$  Hz. The last value corresponds to about 75% of the gain at  $10^4 Hz$ . To illustrate the performance of 85001 MCP PM we show in Fig. 13 two ADC spectra at *very high* counting rate of  $2 \times 10^6$  Hz and ultimate HV of  $2400$  V. Despite of severe conditions both spectra contain a clear peak corresponding to LED signal.

**Number of primary photoelectrons from LED.** It is important to know the energy of the light flash at the input of the PM. We have estimated the number of primary photoelectrons produced by the LED in both MCP PMs. For our measurements of  $N_{ppe}$  we have used ADC spectra obtained at counting rate of  $10^4$  and gain  $\approx 6.5 \times 10^5$ . From several measurements of the peak width (as in Fig. 13) we have estimated the total number of primary photo-electrons produced by LED as  $114 \pm 25$ . This value is close to the  $N_{MIP}$  from Fig. 9.

Therefore, we consider the results shown in Fig. 11 as estimations of the 85001 counting rate capability for minimum ionizing particles.

## 5 Conclusions and Discussion

With two different methods we confirmed that the effective timing resolution of Hamamatsu *R2083*, attached directly to our scintillator, is better than  $60\text{ ps}$ . This value establishes the basis for further studies with  $1\text{ m}$  long light guides, from which we expect the effective resolution to be significantly worse. Therefore, we are looking for alternatives to such a design. With this purpose in mind we have measured the timing resolution for the *Burle* 85001 – 501 MCP PMs. The value of resolution  $130 \pm 4\text{ ps}$  was obtained at the very low gain  $\approx 4.5 \times 10^4$  using an external amplification of  $10^2$  to the PM's signal. We compare these measurements in Table 1.

Method	Acceptance	Particles	$\Delta E$	$\sigma_{PMT}$
6 R2083 tracking	$0 \pm 25\text{ cm}$	cosmic	$4.4\text{ MeV}$	$63.4 \pm 0.6\text{ ps}$
6 R2083 tracking	$\langle local \rangle$	cosmic	$4.4\text{ MeV}$	$59.1 \pm 0.7\text{ ps}$
$X+$ , R2083	$\langle local \rangle$	$\beta$ from $^{90}\text{Sr}$ $E_\beta < 2.28\text{ MeV}$	<i>extrapolated</i> <i>to</i> $\approx 4.4\text{ MeV}$	$59.5 \pm 0.7\text{ ps}$
$X+$ , 85001 MCP PM	$\langle local \rangle$	$\beta$ from $^{90}\text{Sr}$ $E_\beta < 2.28\text{ MeV}$	<i>extrapolated</i> <i>to</i> $\approx 4.4\text{ MeV}$	$130 \pm 4\text{ ps}$

Table 1

PMT resolution(standard deviation) obtained using different methods.  $X+$  stands for the coordinate method extrapolated to MIP energy. The errors shown in this table are obtained by fitting procedures. We estimate a possible systematic error to be of about  $+5\%$  to the shown values.

We emphasize that the results shown in Table 1 were obtained with the prototype, which has no light guides. A good agreement between  $\sigma_{R2083}$ 's from the cosmic ray method (6 *PMT* tracking) and coordinate method with extrapolation to higher energies ensures that coordinate method is an adequate tool for measuring of  $\sigma_{PMT}$  at MIP energy.

Another important parameter of MCP PM is its counting rate capability, which was also addressed in our studies. We have shown that at low MCP

gain the counting rate of MIPs can be as high as  $0.5 \times 10^6$ .

The resolution is dictated mostly by fluctuations of primary electrons. Within coordinate method we have estimated the number of primary photo-electrons caused by MIPs in MCP. This number is 2.7 times lower than the value expected from the *Burle* – 85001 data sheet. However, the same method of estimating the number of primary photo-electrons gives the reasonable value for the *R2083* PMs of Hamamatsu. Therefore, we believe that the resolution of the *Burle* – 85001 MCP PM should improve by  $\approx 1.6$  to about 80 ps provided the number of primary photoelectrons corresponds to the data sheet for the 85001 photo-cathode. In that case the timing resolution of *Burle*–85001 would come significantly closer to the requirements of CLAS experiments at 12 GeV. Its current counting rate capability ( $0.5 \times 10^6$ ) with external amplification of  $10^2$  is also quite close to the typical counting rates of CLAS experiments. Nevertheless, we believe that both the resolution and counting rate capability of MCP PMs has to be improved. The progress could be achieved via implementation of Wide Dynamic Range MCPs such as F6584 from Hamamatsu. Photo-multipliers instrumented with WDR MCPs could operate at significantly higher counting rates and/or gains, and resolution, as well. Therefore, we encourage PMT manufacturers to develop such photo-multipliers.

## Acknowledgements

The Southeastern Universities Research Association (SURA) operates the Thomas Jefferson National Accelerator Facility for the United States Department of Energy under contract DE-AC05-84ER40150. This work was also supported in part by the Korea Research Foundation.

## References

- [1] Jefferson Lab 12 GeV Upgrade Project, <http://www.jlab.org/12GeV/>.
- [2] E.S.Smith *et al.*, Nucl. Instr. and Meth. **A432** (1999) 265.
- [3] B.A.Mecking, *et al.*, Nucl. Instr. and Meth. **A 503** (2003) 513.
- [4] R.T.Giles, F.M.Pipkin, J.P.Wolinsky, Nucl. Instr. and Meth. **A252** (1986) 41.
- [5] H. Kichimi *et al.*, Nucl. Instr. and Meth. **A325** (1993) 451.
- [6] V.N. Batourine *et al.*, “Measurements of PMT time resolution at Kyungpook National University,” CLAS-NOTE 2004-16, February, 2004.
- [7] V. Popov, Nucl. Instr. and Meth. **A505** (2003) 316.

Fig. 1. Experimental setup and electronics circuit diagram; 1-passive splitter, 2-constant fraction discriminator, 3-fanout, 4-gate generator.

Fig. 2. The “ $\beta$ -ray” images of  $^{90}\text{Sr}$  source in two energy intervals of  $\beta$ -particles. Top panel:  $E_\beta < 1.2 \text{ MeV}$ . Bottom panel:  $E_\beta > 1.2 \text{ MeV}$ .

Fig. 3. Coordinate method for Hamamatsu *R2083* at  $^{90}\text{Sr}$  location  $-15\text{ cm}$ . Panel top-left: - energy ( $E$ ) spectrum of  $\beta$ -particles ; bottom-left: coordinate( $X$ ) spectrum of  $\beta$ -particles; top-right:  $\sigma_X$  of the peak vs  $\beta$ -particle energy( $E$ ); bottom-right:  $\langle X \rangle$  of the peak vs  $\beta$ -particle energy( $E$ ). The peak position on the  $X$ -scale was adjusted to zero for convenience.

Fig. 4. Top-left: energy ( $E$ ) spectrum of  $\beta$ -particles; top-right: energy dependence of the number of primary photoelectrons  $N_{ppe}(E)$ . It is s expected to be  $685 \pm 10$  at MIP energy of  $\approx 4.4 MeV$ ; bottom-left: spectrum of  $(e_l - e_r)$ , where  $e_{l,r}$  are the energies measured from two sides of the counter; bottom-right: mean value of  $(e_l - e_r)$  vs energy ( $E$ ) of  $\beta$ -particles.

Fig. 5. The dependence of  $\sigma_{PMT}$  yielded by the coordinate method upon the signal amplitude  $A_s$ , which was measured with the scope. The mean value of  $\sigma_{PMT}$  in the plateau region (0.9, 1.8 V) is of  $59.5 \pm 0.7$  ps. The curve represents the fit by  $P1/A_s + P2$ .

Fig. 6.  $\sigma_{PMT}$  vs  $x$ -coordinate at voltages 2.37 and 2.5  $kV$  on the left and right PM, respectively. The mean value is  $59.5 \pm 0.7$   $\mu s$ .

Fig. 7. Effective PMT resolution from the three counter method. Top-left: scatter plot of 6 PMT residuals  $\delta t$  vs  $X$ ; top-right: distribution of 6 PMT residuals ( $\delta t$ ), which yields the overall  $\sigma_{PMT} = 63.4 \pm 0.6$  ps; bottom-left: second moment of residuals  $\sigma$  vs  $X$ , which yields the local  $\sigma_{PMT} = 59.1 \pm 0.7$  ps as mean value; bottom-right: First moment of  $\delta t$  distribution  $X^0$  vs  $X$ .

Fig. 8. Coordinate method with MCP PM from “Burle” at highest  $HVs = (2150 V, 2400 V)$ . Extrapolated to MIPs  $\sigma_{PMT}$  is of  $125 \pm 4 ps$ . Amplification factor is of  $10^1$ .

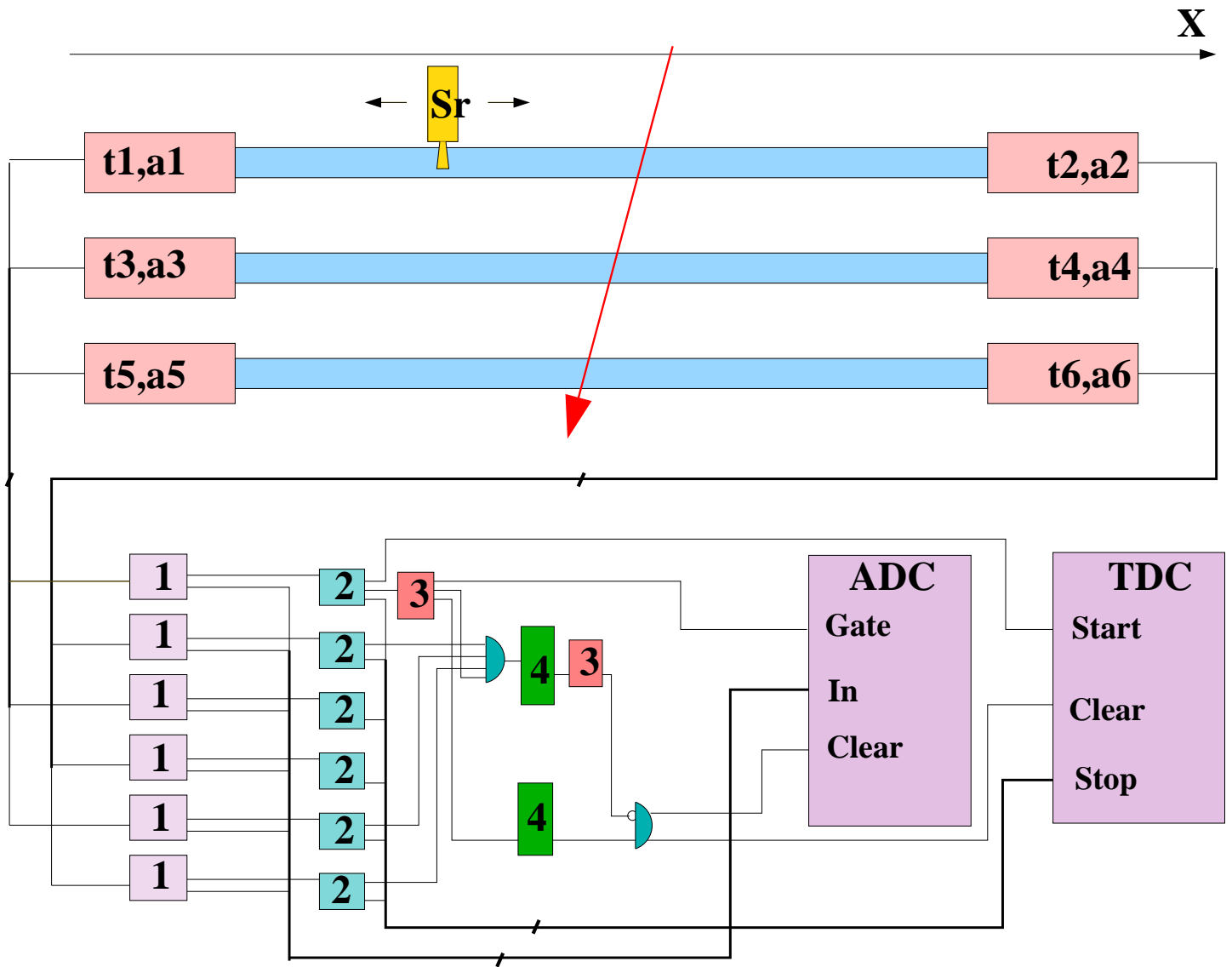
Fig. 9. Coordinate method with MCP PM from “Burle” at  $HVs = (1940, 2100) V$ . Extrapolated to MIPs  $N_{ppe}=127 \pm 10$ . Amplification factor is of  $10^2$ .

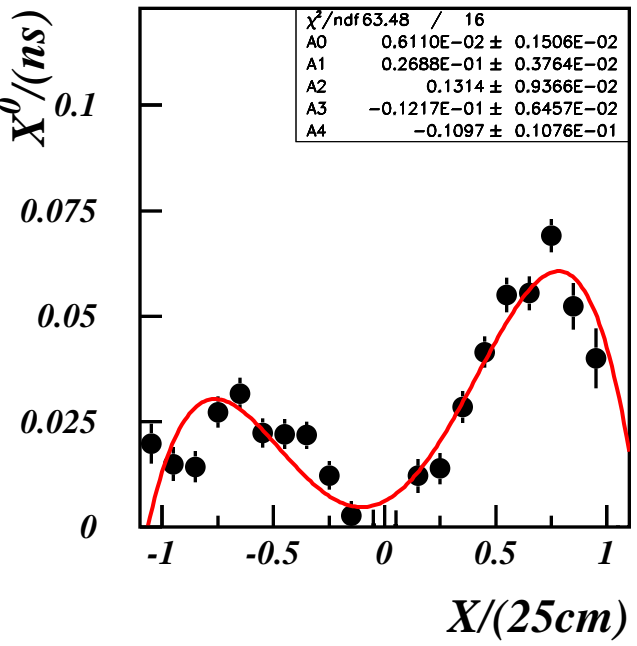
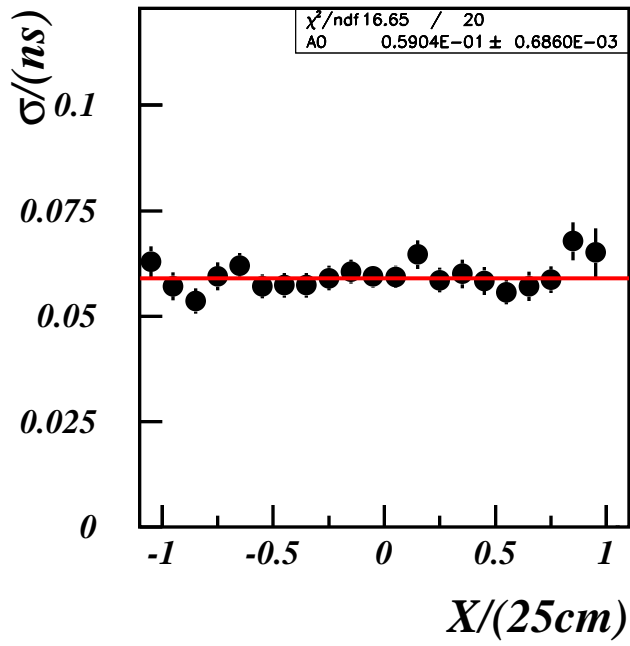
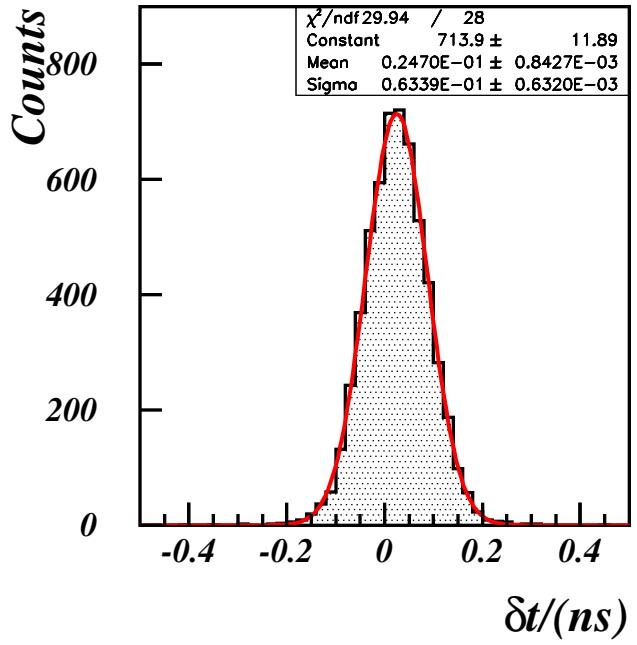
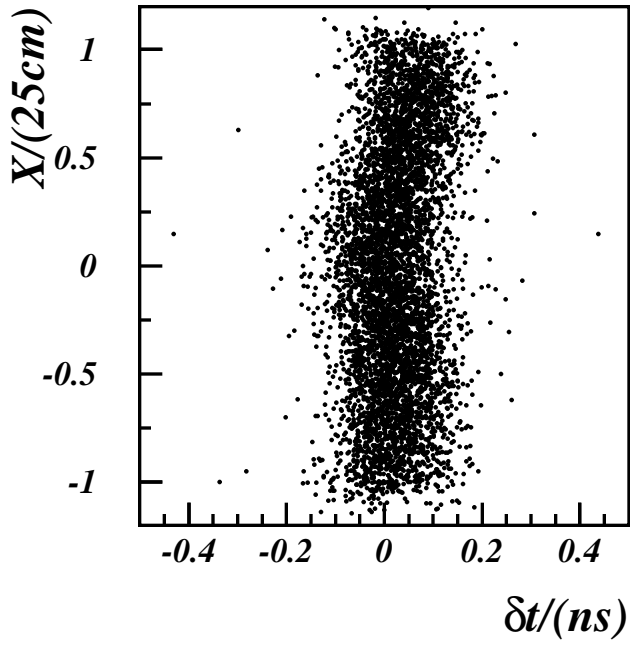
Fig. 10. High Voltage vs MCP Gain. The curves (1) and (2) are fits to the power law. (1)-left MCP PM,(2)-right MCP PM.

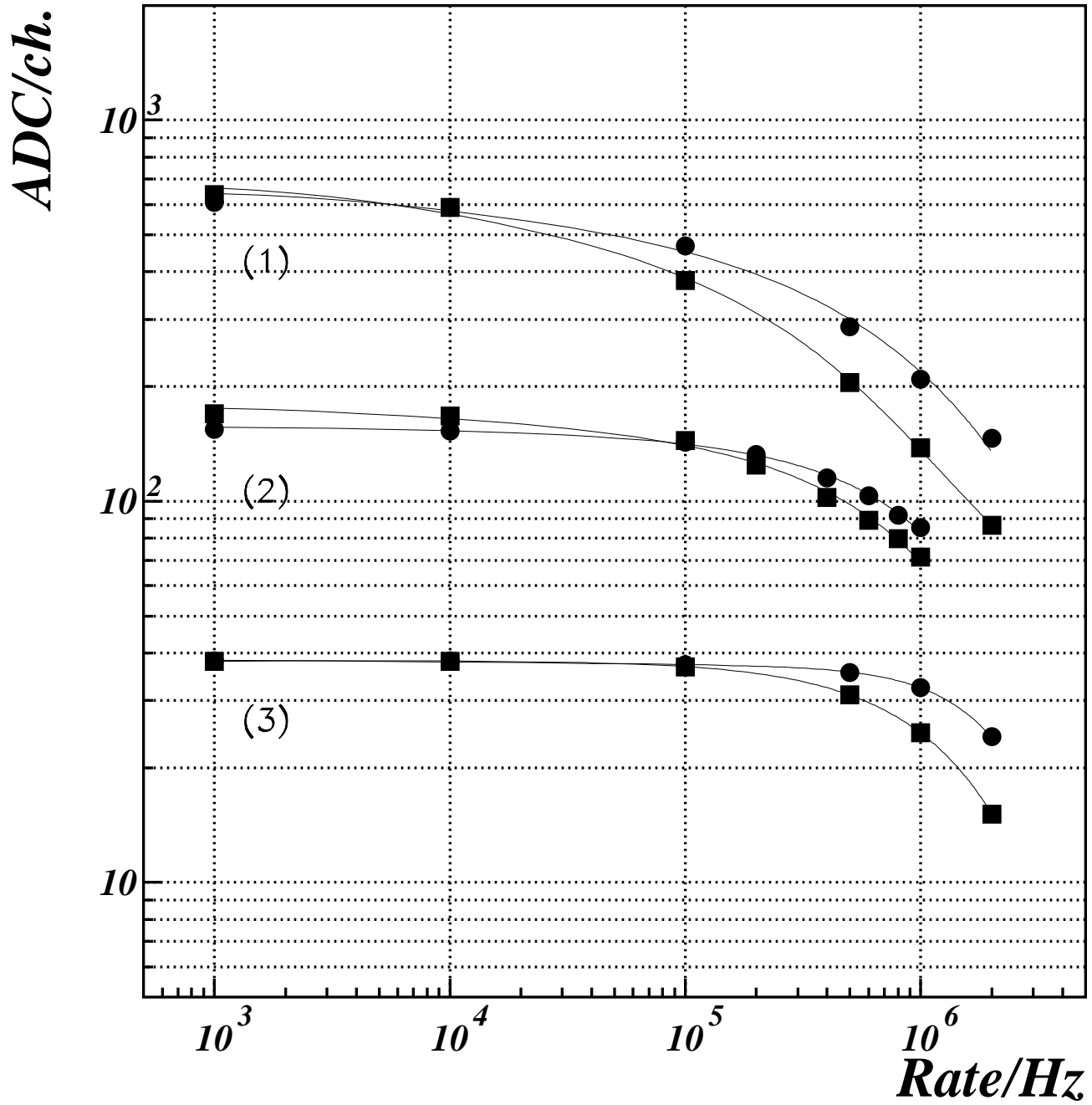
Fig. 11. Resolution vs MCP gain( $G$ ). Squares are for  $\sigma_{PMT}$  at  $\Delta E = 2.28 \text{ MeV}$ . Circles are for  $\sigma_{PMT}$  extrapolated to  $\Delta E = 4.4 \text{ MeV}$ (MIPs) The curves are fits to the  $G^{-2}$  dependence. Amplification factor varies from 10 in the gain region of  $(2.0, 6.5) \times 10^5$ (white symbols) to  $10^2$  in the region  $(0.13, 2.0) \times 10^5$ (black symbols). Two points at  $2.0 \times 10^5$  were measured at amplification  $10^1$  and  $10^2$  for comparison.

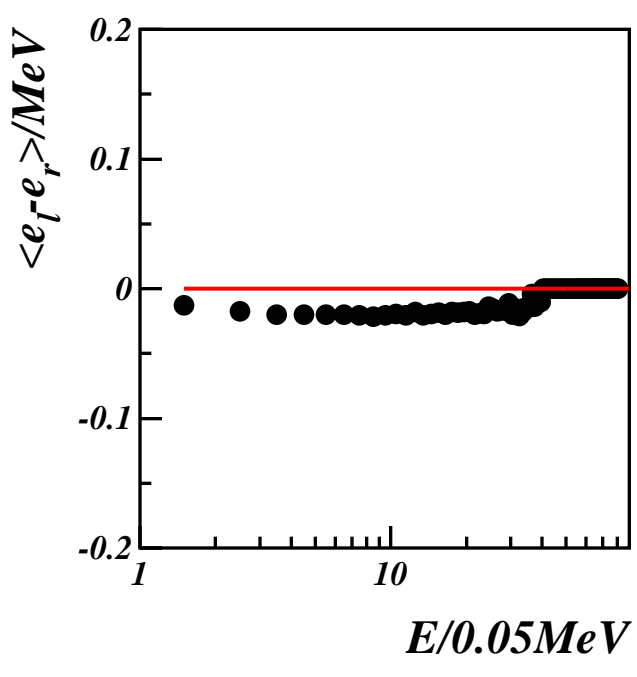
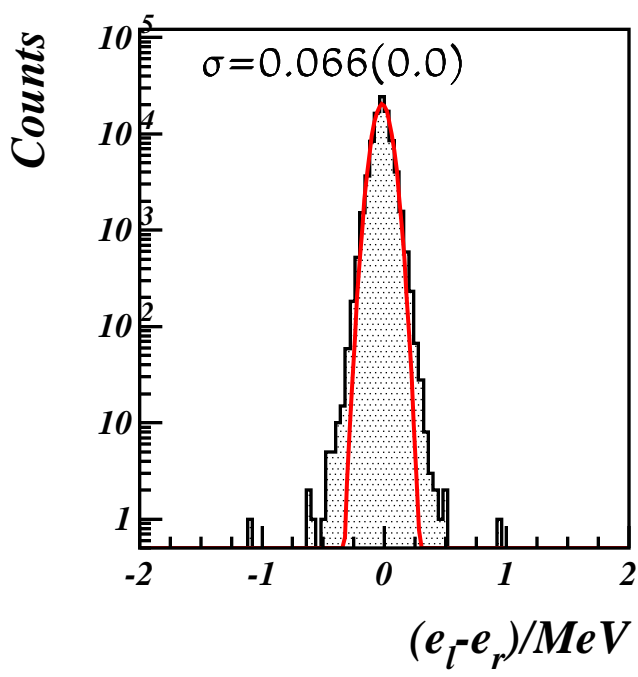
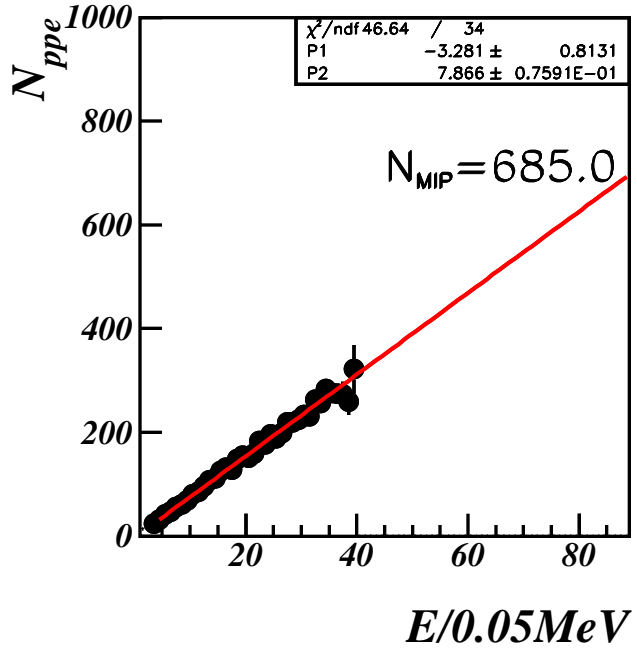
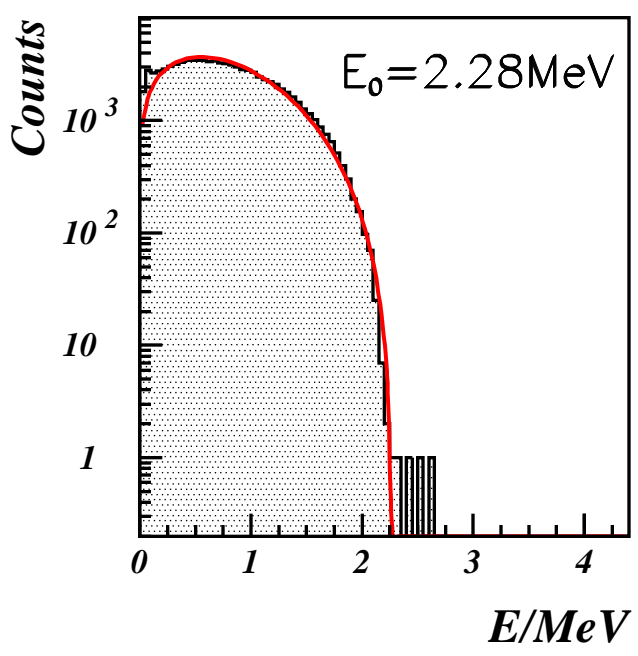
Fig. 12. The integrated current of MCP PM signal (ADC counts) vs the rate of light flashes at: (1) HVs=(2400, 2400) V and  $\tau = 100$  ns; (2) HVs=(2400, 2400) V and  $\tau = 50$  ns; (3) HVs=(1815, 1875) V and  $\tau = 100$  ns. Amplification factor is  $10^2$  (two cascaded amplifiers). The light has been generated by the LED fed with the pulser.

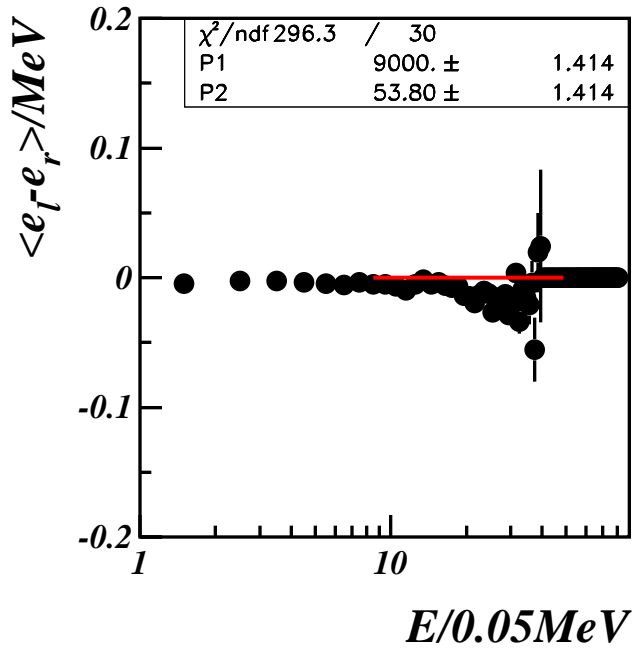
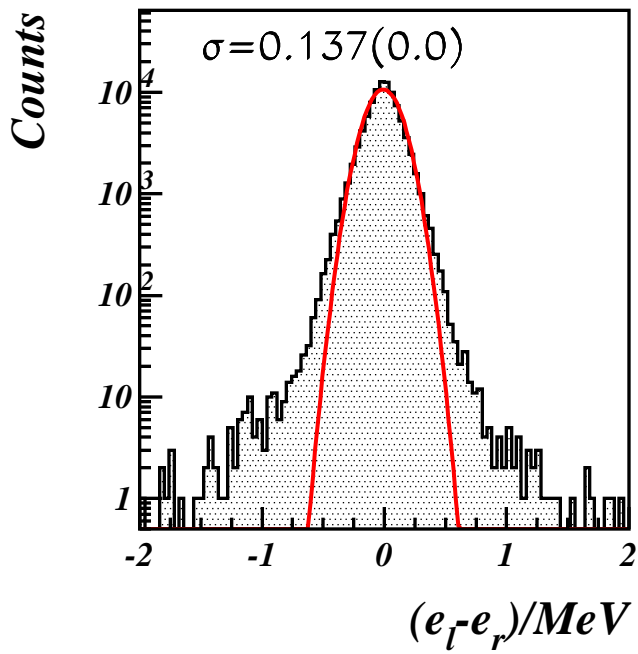
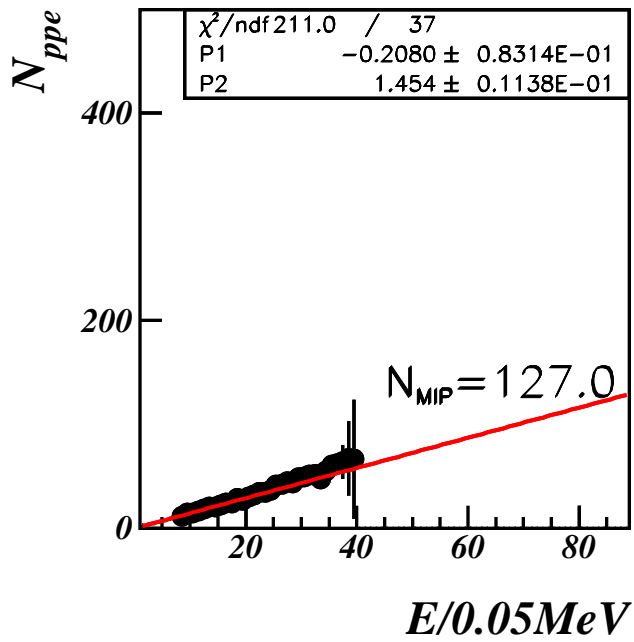
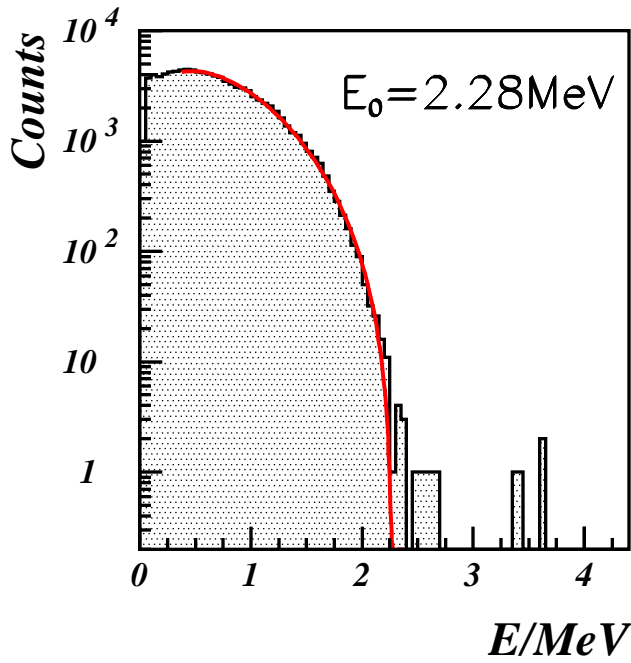
Fig. 13. The pedestal subtracted ADC spectra of signals from LED operating at  $2\text{ MHz}$  rate. The amplification to MCP signals is  $10^2$ , HV is  $2.4\text{ kV}$  for both PMs.

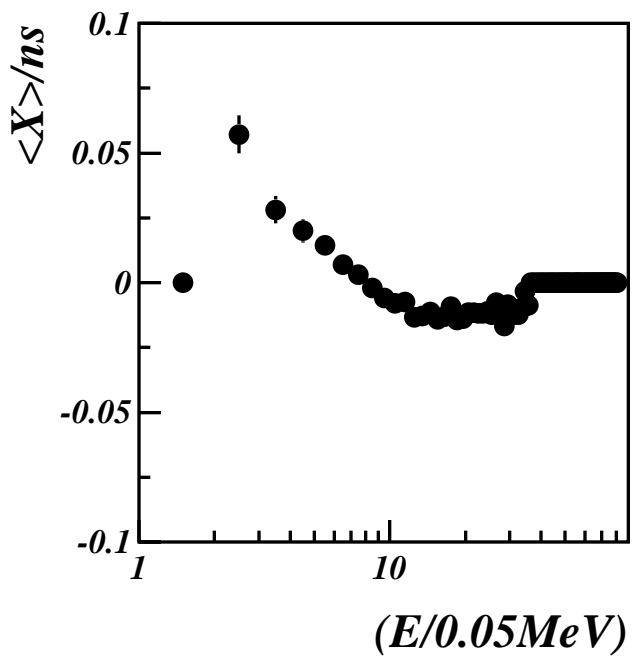
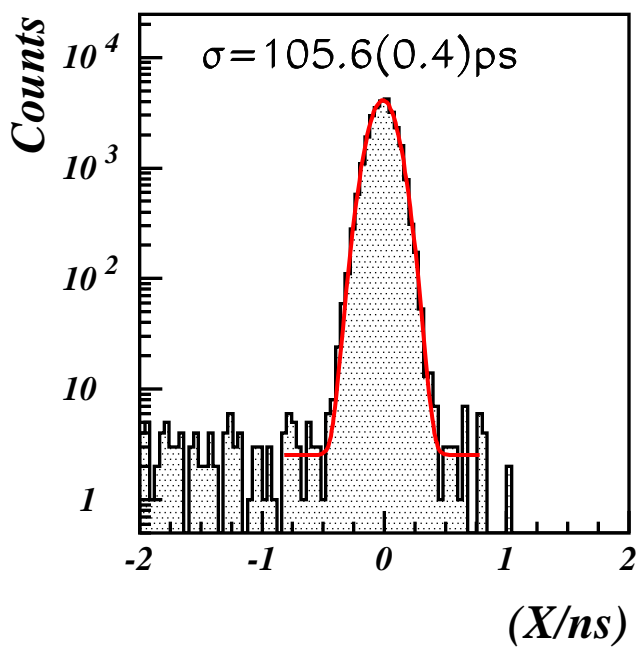
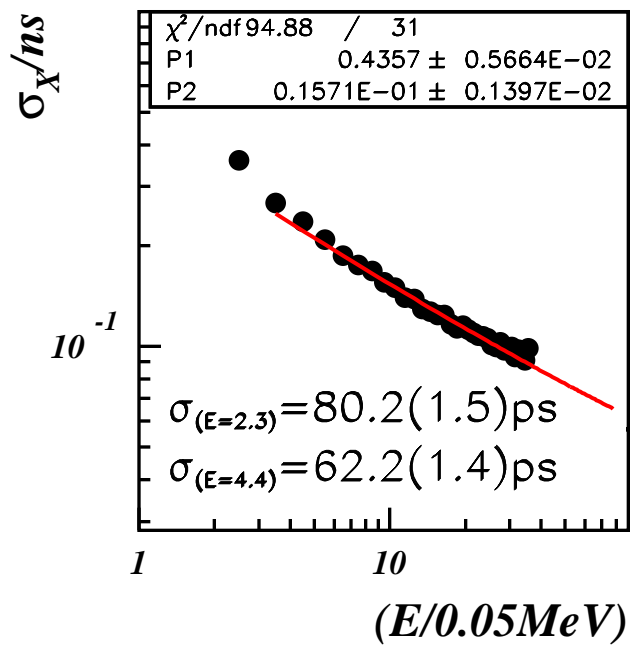
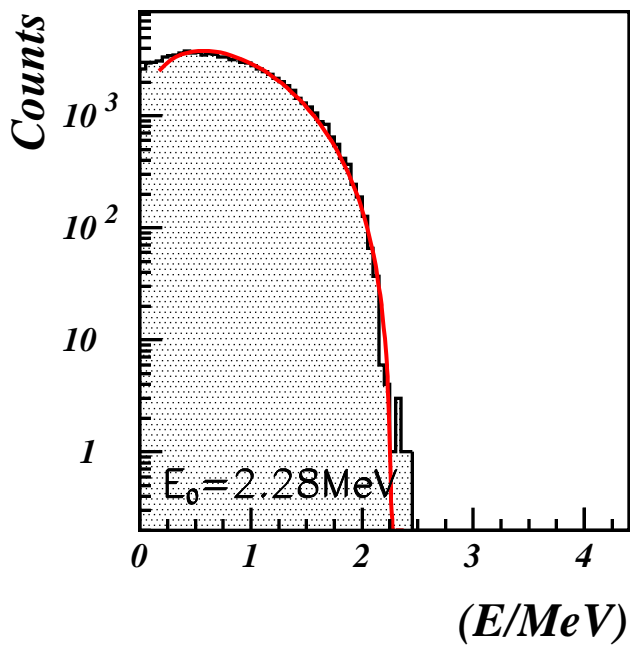


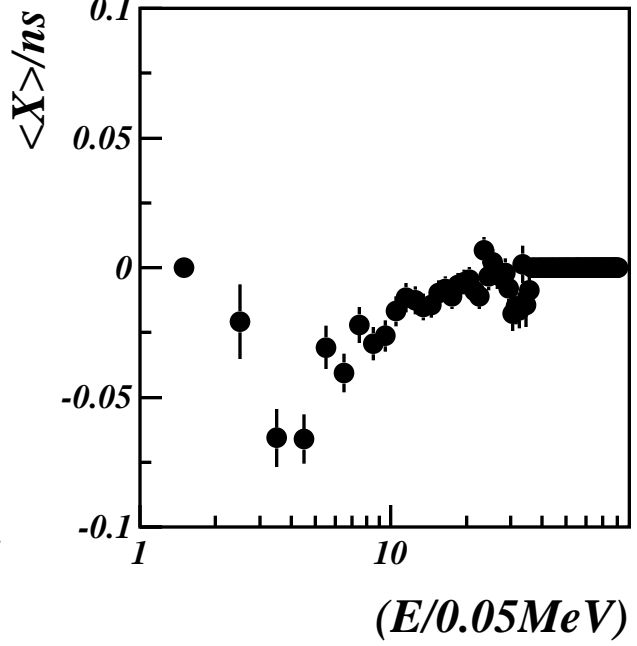
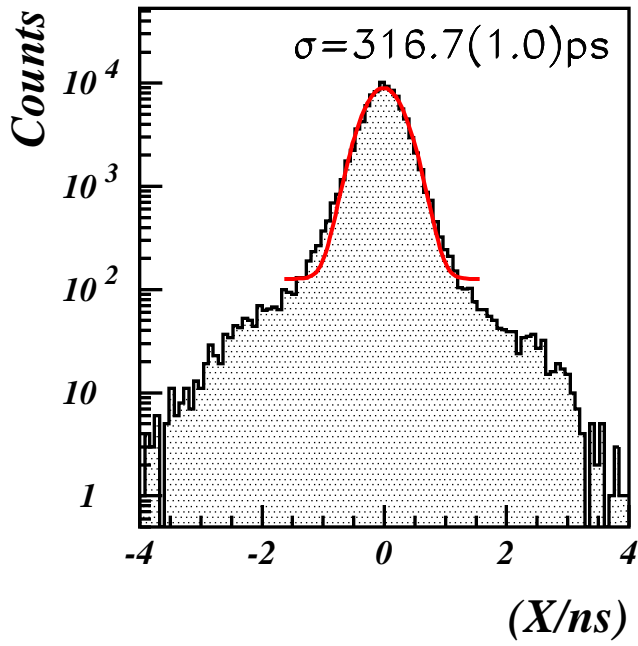
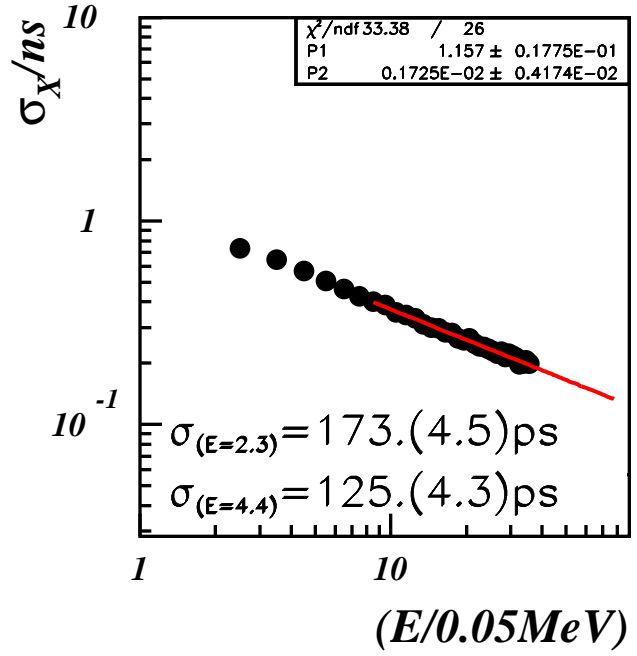
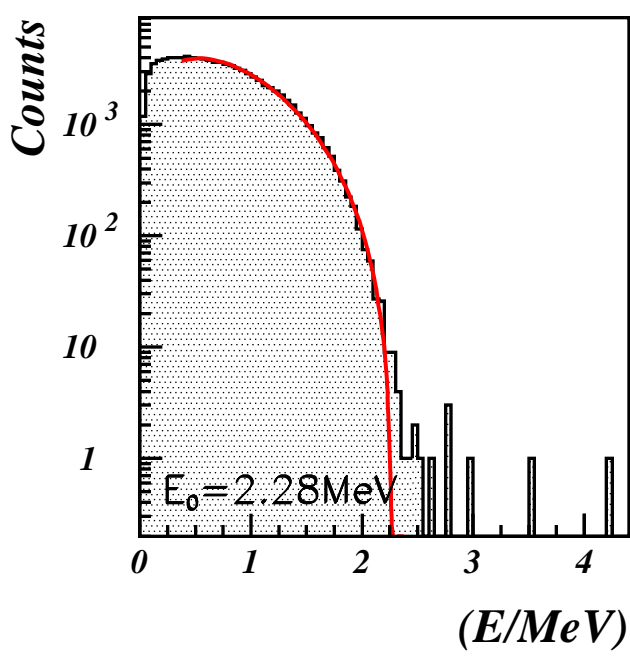


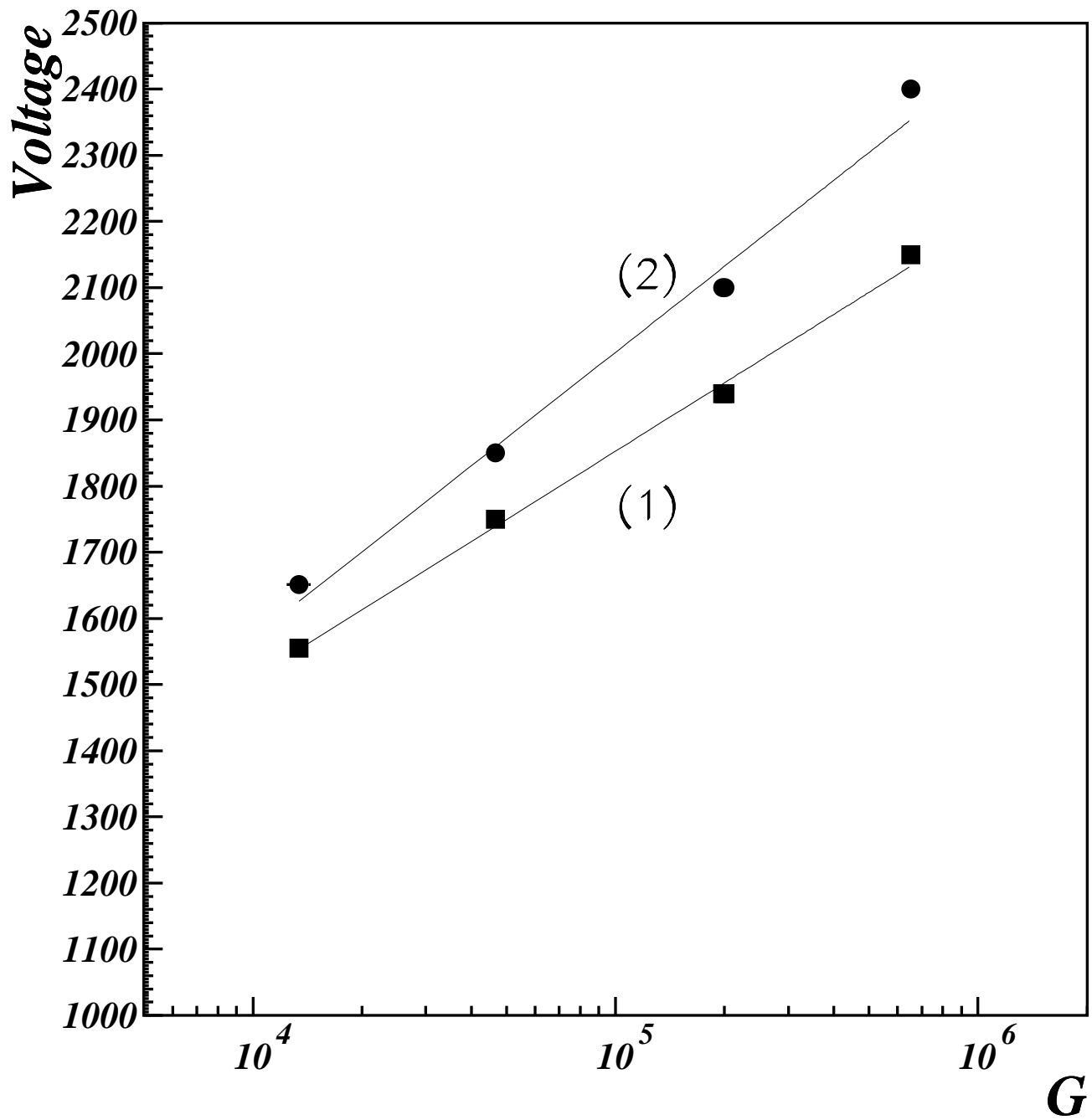


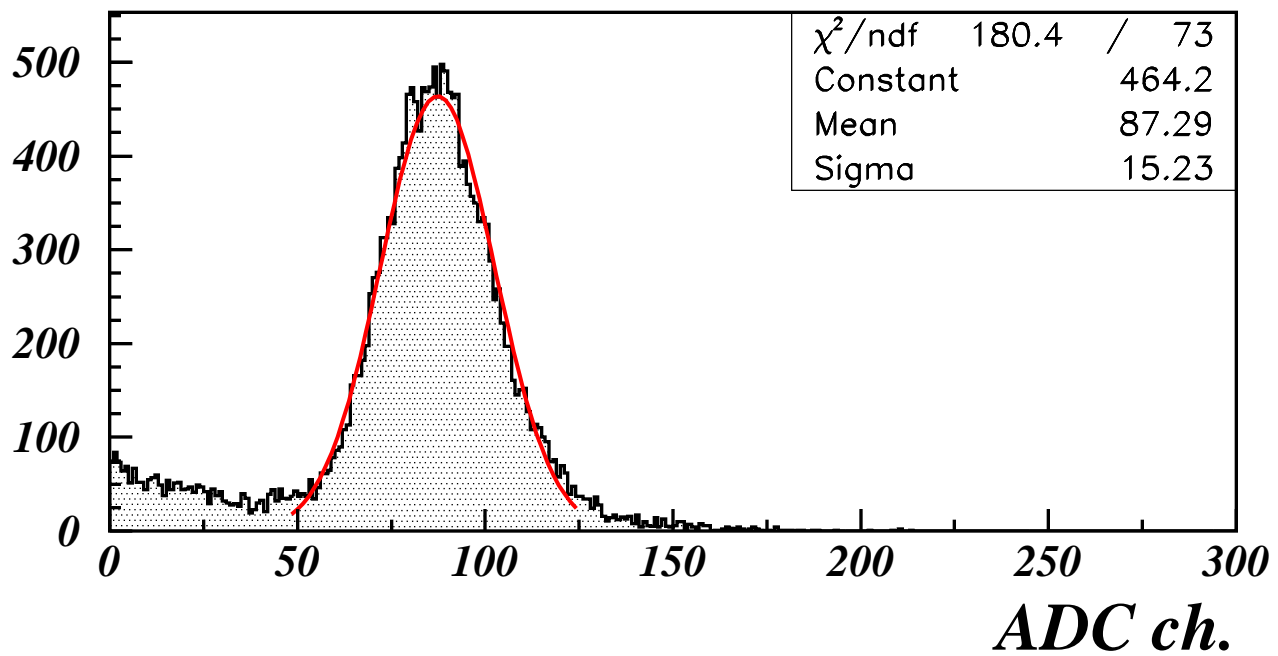
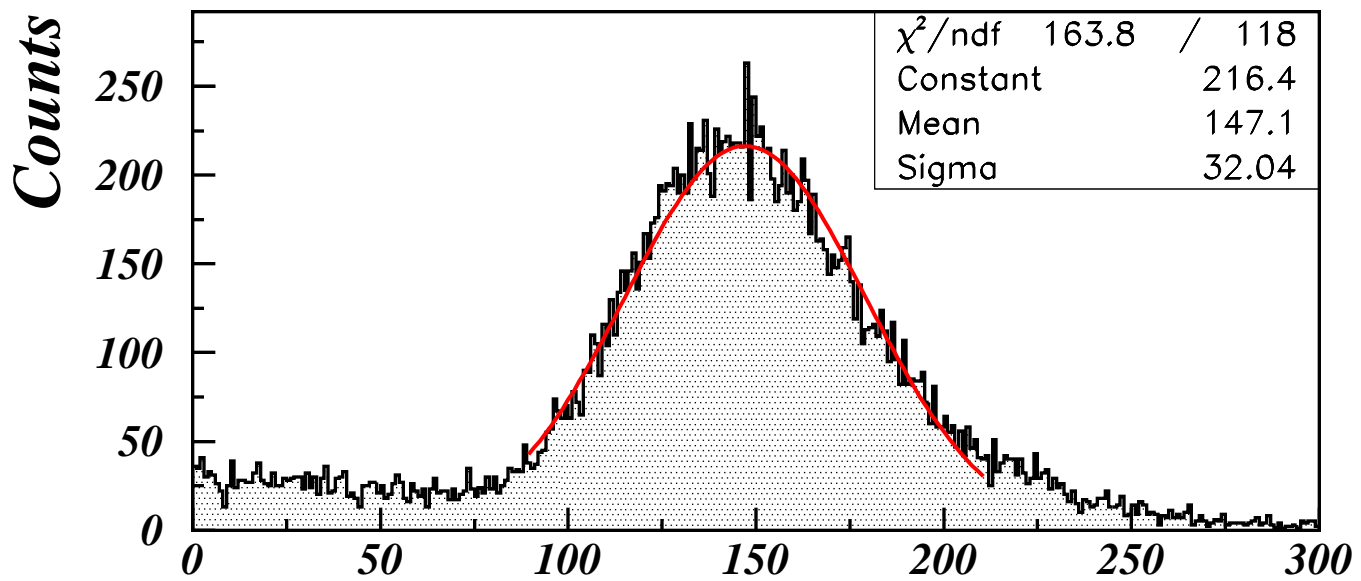


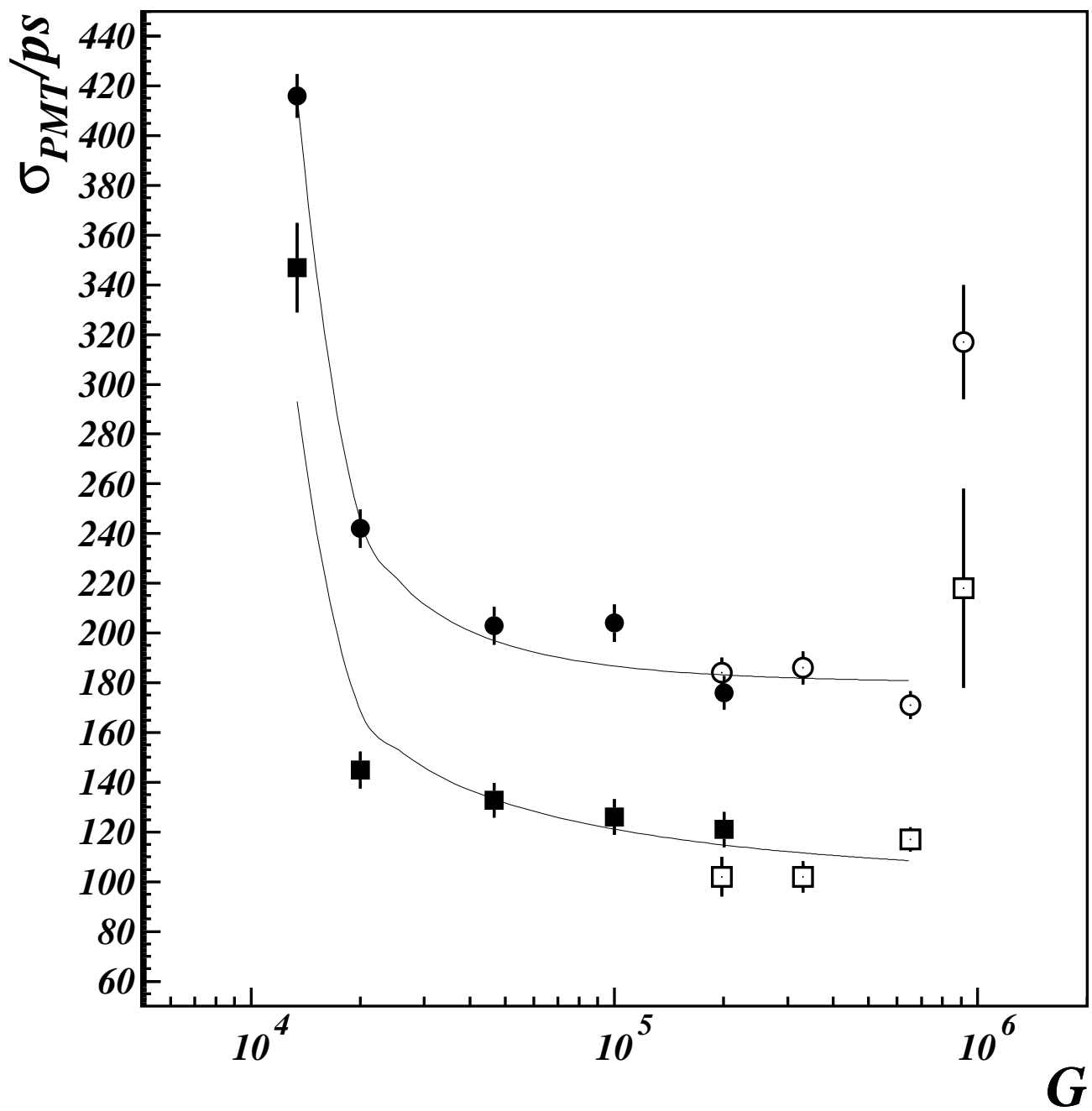


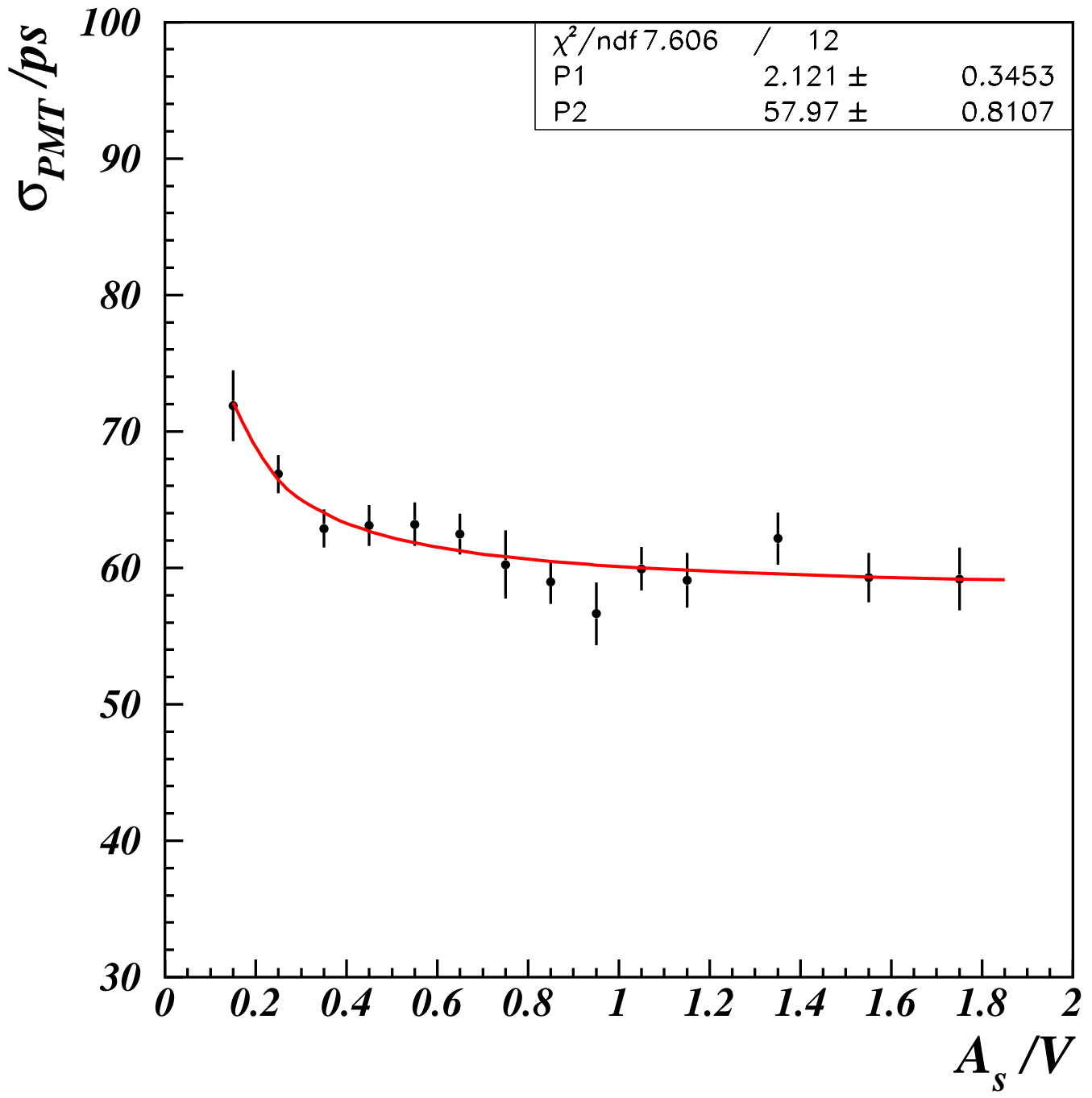


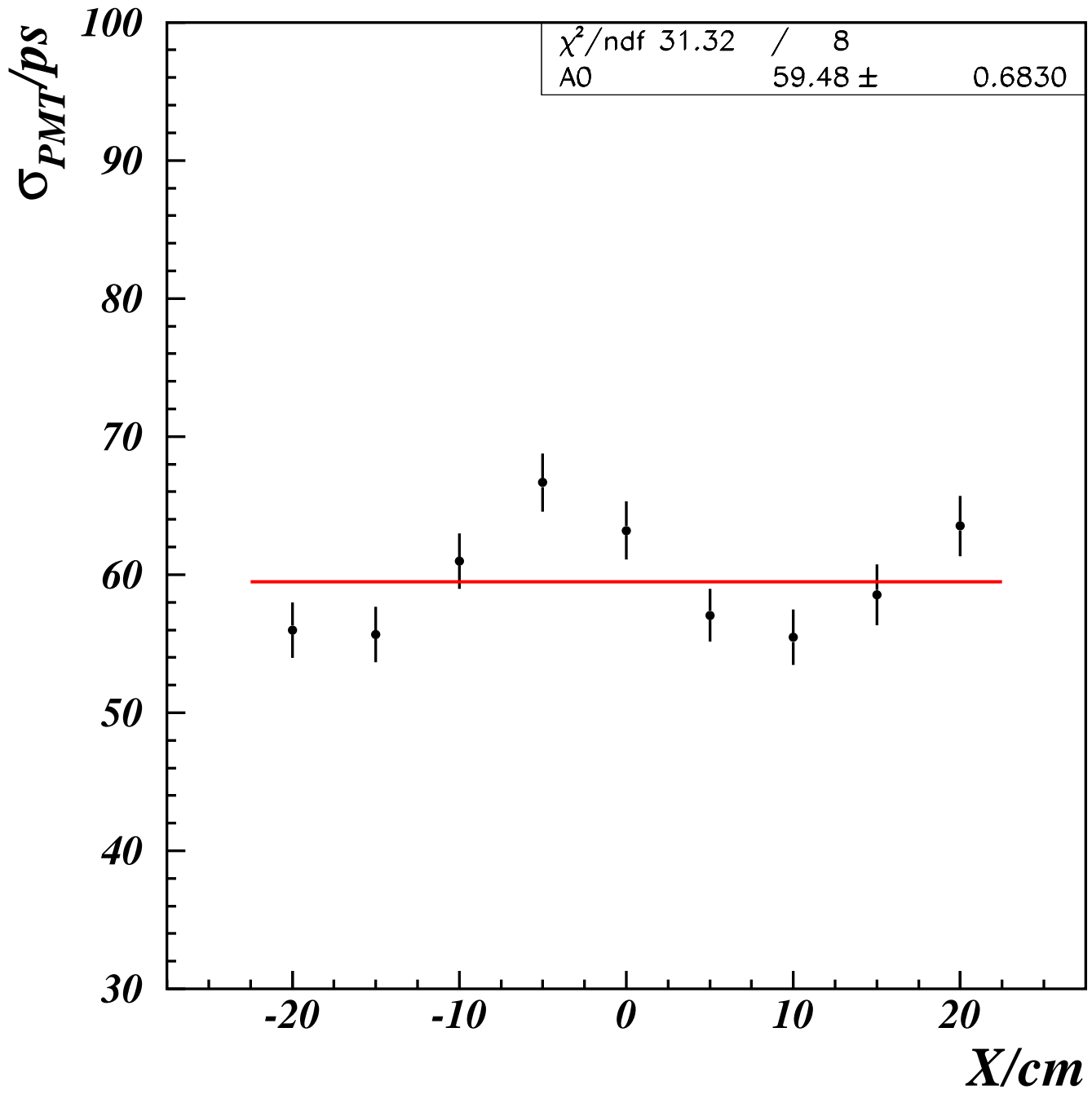


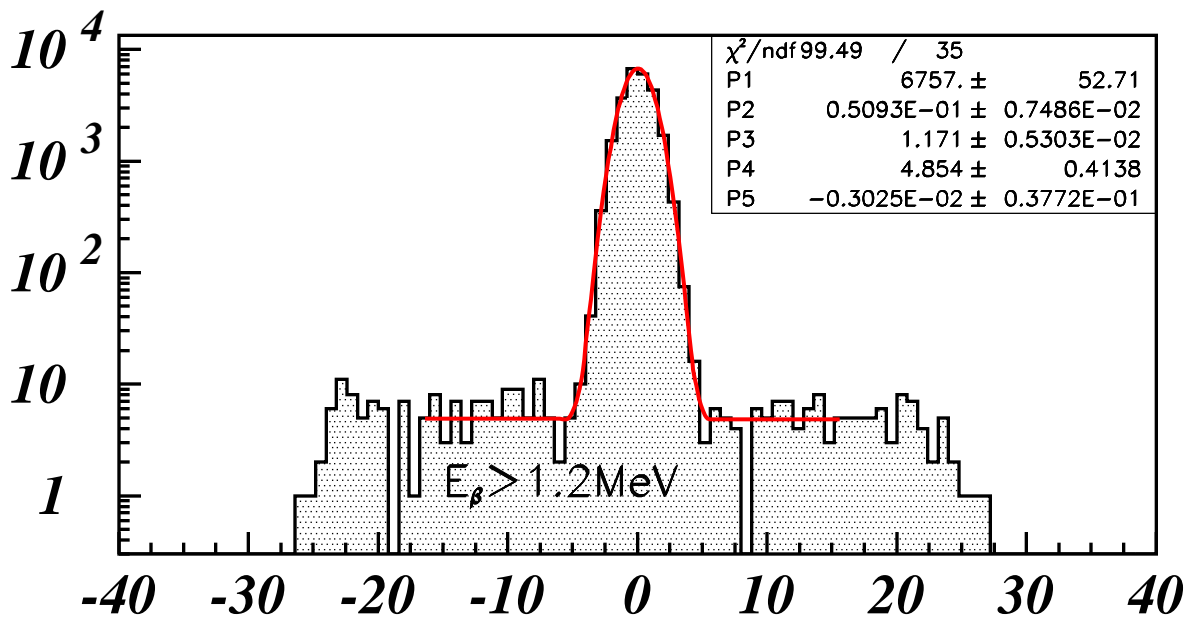
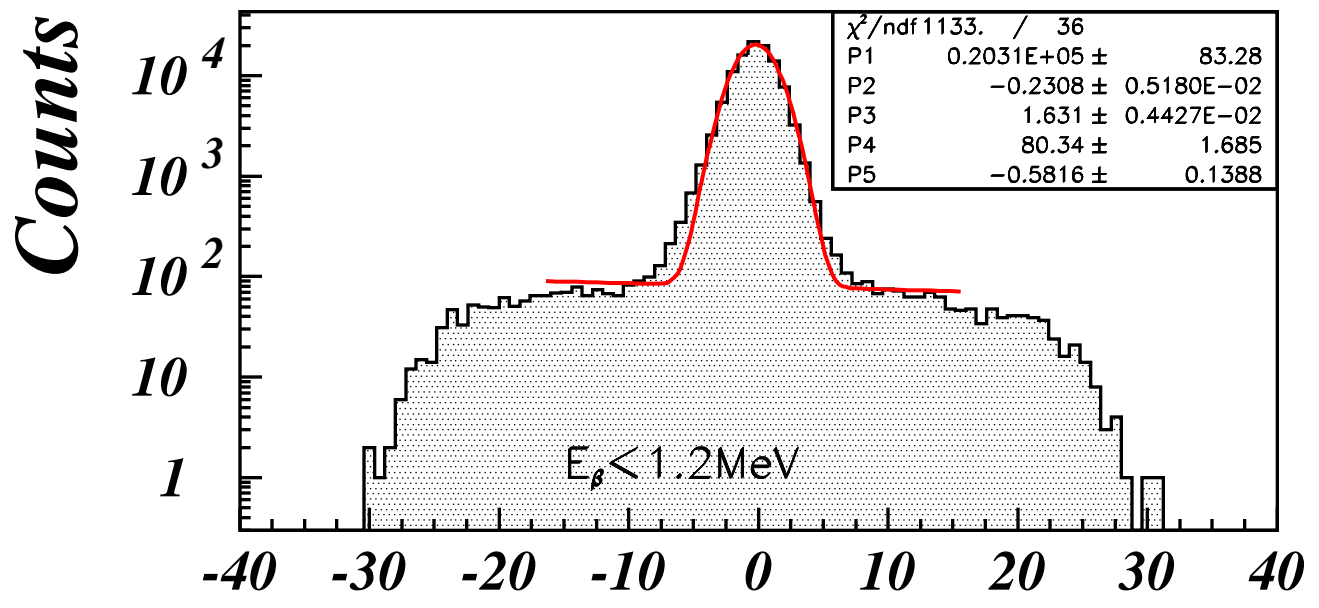












***X(cm)***